Available online at www.sciencedirect.com
SCIENCE DIRECT®
International Journal of Heat and Mass Transfer 47 (2004) 3387–3401
International Journal of HEAT and MASS TRANSFER
www.elsevier.com/locate/ijhmt

Heat transfer model for evaporation in microchannels. Part II: comparison with the database

V. Dupont [a], J.R. Thome [a,*], A.M. Jacobi [b]

[a] Laboratory of Heat and Mass Transfer (LTCM), Faculty of Engineering Science, Swiss Federal Institute of Technology Lausanne (EPFL), CH-1015 Lausanne, Switzerland

[b] Department of Mechanical and Industrial Engineering, University of Illinois at Urbana-Champaign, Urbana 61801, USA

Received 15 September 2003; received in revised form 19 January 2004
Available online 20 March 2004

Abstract

In part I, a *three-zone* flow boiling model is formulated to describe evaporation of elongated bubbles in microchannels. The heat transfer model describes the transient variation in local heat transfer coefficient during the sequential and cyclic passage of (i) a liquid slug, (ii) an evaporating elongated bubble and (iii) a vapor slug. In this part, the time-averaged local heat transfer coefficient is compared to experimental data taken from seven independent studies covering the following seven fluids: R-11, R-12, R-113, R-123, R-134a, R-141b and CO_2. The 1591 test data cover tube diameters from 0.77 to 3.1 mm, mass velocities from 50 to 564 kg/m^{2}s, pressures from 124 to 5766 kPa, heat fluxes from 5 to 178 kW/m^2, and vapor qualities from 0.01 to 0.99. The new model predicts 67% of the database to within ±30%. The new model illustrates the importance of the strong cyclic variation in the heat transfer coefficient and the strong dependency of heat transfer on the bubble frequency, the minimum liquid film thickness at dryout and the liquid film formation thickness.

1. Heat transfer database presentation

The heat transfer database drawn together for this study is described in Table 1. Local heat transfer data were taken from seven different publications [1–8] obtained at six different laboratories for seven fluids, all for circular cross-sectional tubes. All of these results are for a single flow channel except for that of Yan and Lin [4] and Agostini [8], which are for test channels with multiple channels. As most of the results are for low to intermediate vapor qualities, it will be assumed here that all these data fall in the elongated bubble regime. A total of 1591 experimental points are in the database. All data were obtained from digitalizing published graphs, with the exception of Bao et al. and Baird et al., who kindly provided computer files. The individual studies are described briefly below.

The first such study found was that of Lazarek and Black [1], who investigated evaporation of R-113 in a 3.1 mm stainless tube. They performed experiments starting from subcooled inlet conditions with a two-part vertical test section heated by direct current. Fig. 1 depicts their data (note: the predictions by the new model shown will be discussed later). The results show a strong dependence of the saturated boiling heat transfer on heat flux but a negligible influence of quality, which suggested to them that the nucleate boiling was controlling heat transfer. Only 13 data points were measured, thus the weight of this study is not important in the database.

Next, in a systematic study at Argonne Laboratory by Wambsganss et al. [2], further results for R-113 evaporating in a circular channel of 2.92 mm diameter were presented (Fig. 2) while another later study at the same laboratory by Tran et al. [3] reported results for R-12 evaporating in a 2.46 mm circular channel (Fig. 3).

* Corresponding author. Tel.: +41-21-693-5981; fax: +41-21-693-5960.
E-mail address: john.thome@epfl.ch (J.R. Thome).

0017-9310/$ - see front matter © 2004 Elsevier Ltd. All rights reserved.
doi:10.1016/j.ijheatmasstransfer.2004.01.007

Nomenclature

Boi	Boiling number, dimensionless
Co	Confinement number, dimensionless
$C_{\delta 0}$	correcting factor on the initial film thickness, dimensionless
d, d_h	diameter, hydraulic diameter, m
f	pair frequency, Hz
G	mass velocity, $kg\,m^{-2}\,s^{-1}$
h	heat transfer coefficient, $W\,m^{-2}\,K^{-1}$
J	objective function, $W^2\,m^{-4}\,K^{-2}$
n_f	exponent, dimensionless
P	pressure, Pa
q	heat flux, $W\,m^{-2}$
Ra	average roughness, m
U	velocity, $m\,s^{-1}$
x	vapor quality

Greek symbols

α_q	coefficient in Eq. (3), $W\,m^{-2}$
δ	liquid film thickness, m
ΔT_{sat}	superheat of the wall, K
λ	thermal conductivity, $W\,m^{-1}\,K^{-1}$

Subscripts

crit	thermodynamic critical point
end	end of the liquid film
exp	from experiment
film	liquid film
l	liquid
min	minimum
model	from the model
opt	optimum value
p	pair
ref	reference
sat	saturation
v	vapor
w	wall
0	initial

They used a test section heated by direct current and the liquid enters subcooled. Wambsganss et al. [2] gave a complete description of the test set-up and the diameter of the tube is near the maximum value of the database at the limit of the mesotube classification. In Tran et al. [3], the experimental test section was electrically heated with four clamps in order to change the heated length. After each clamp a thermocouple measured the bulk temperature of the fluid. The perturbation of the channel wall by a probe (a hole or solder) could promote bubble nucleation at the wall at this point and thus change the bubble formation frequency. Fig. 2 shows some of their results with heat transfer plotted vs. vapor quality for R-12 at various heat fluxes and mass velocities. In general, at wall superheats larger than 2.75 K, they noted that the local heat transfer coefficients did not change with mass velocity (over the range from 50 to 695 kg/m^{2}s) nor with vapor quality (from 20% to 75%) but were dependent on heat flux (from 7.5 to 59.4 kW/m^2). Consequently, applying macroscale logic, they concluded that heat transfer was always nucleate-boiling dominated in microchannel evaporation and fit their data to a nucleate boiling curve (of the form $q = a\Delta T^n$ where ΔT is the wall superheat and q is the heat flux), obtaining an exponent of $n = 2.7$ typical to nucleate pool boiling correlations. At lower superheats (below 2.75 K), not shown here, they observed a significant change in the slope of their data plotted as a nucleate boiling curve (q vs. ΔT), and this behavior they designated as a convection-dominant regime (even though it was still heat flux dependent).

Yan and Lin [4] investigated flow boiling of R-134a inside a bundle of 28 pipes with a inside diameter of 2 mm. These tubes were soldered (sandwich style) between two copper plates of 5 mm thickness. Thin electrical heaters were installed on the external side of the plates. This set of tests is the only one in the database where a preheater has been used to control the vapor quality at the inlet of the test section. Unfortunately, the diameter of the tube of the preheater and the heat flux associated are unknown at the location where the bubbles were created. In this study, the mass flux was varied from 50 to 200 kg/m^{2}s, heat flux from 5 to 20 kW and saturation temperature from 5 to 31 °C. The results show (Fig. 4) a vapor quality dependence. Usually heat transfer increased with heat flux but this trend was inverted at high vapor quality (approximately above $x = 0.6$). The authors gave a correlation to predict these evaporation coefficients, which was corrected later in Webb and Paek [9]. The test section is multichannel and the authors verified the uniformity of the mass flow in single-phase flow but it is not obvious that this uniformity still persists when circulating a two-phase flow. Furthermore, the heating configuration increased the thermal inertia of the wall.

Zhao et al. [10] reported flow-boiling coefficients for CO_2 and R-134a in a microchannel for vapor qualities from 5% to 30%. For mass velocities from 250 to 700 kg/m^{2}s at fixed heat fluxes, no mass-flux dependence was observed on the flow boiling heat transfer coefficients for either CO_2 or R-134a for pressures ranging from 4.0 to 5.1 bar and 0.35 to 0.49 bar, respectively. In their heat flux range (8–25 kW/m^2), their results did not show any *heat flux* dependence, in contrast to the studies discussed above. These tests were for small wall superheats (1–2

Table 1
Database used to perform parameter identification

Study	Fluid	d_h [mm]	G [kg m^{-2} s^{-1}]	q [kW m^{-2}]	P_{sat} [kPa]	x [-]	Uncertainties in h	Data points	Remarks
Lazarek and Black [1]	R113	3.1	502	114–178	170	0.03–0.61	5%	13	Circular single tube
Wambsganss et al. [2]	R113	2.92	50–300	124–160	124–160	0.01–0.88	0.2 K[a]	92	Circular single tube
Tran et al. [3]	R12	2.46	63.3–300	7.5–59.4	825	0.2–0.77	6–18%	60	Circular single tube
Yan and Lin [4]	R-134a	2	50–200	2–20	350–793	0.08–0.93	6%	125	Multichannels with 28 circular channels
Bao et al. [5]	R11	1.95	167–564	9.8–176.6	214–477	0.01–0.98	5%	299	Circular single tube
Bao et al. [5]	R123	1.95	167–452	36.2–131	346–509	0.02–0.85	5%	126	Circular single tube
Baird et al. [6]	CO_2	1.95	68–266	2.6–48.4	4057–5733	0.01–0.74	?	379	Circular single tube
Lin et al. [7]	R141b	1.1	510	18–72	134–219	0.01–0.99	0.5 K[a]	92	Circular single tube
Agostini [8]	R-134a	0.77 & 2.01	117–347	5.2–26.4	405–600	0.01–0.95	5–30%	405	Multichannels with 11 and 18 rectangular channels

[a] Uncertainties on temperature measurement.

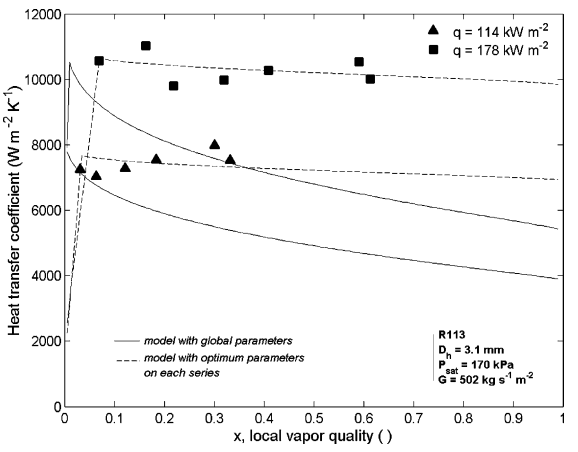

Fig. 1. Lazarek and Black [1] results with R-113 in 3.1 mm tube.

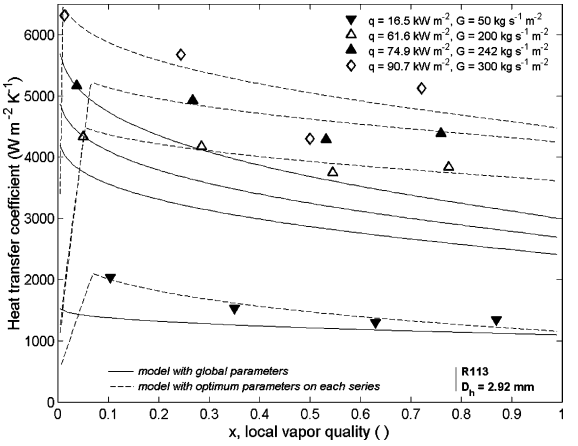

Fig. 2. Flow boiling data for R-113 in 2.92 mm tube of Wambsganss et al. [2].

K) and hence would have fallen in the lower heat-flux dependence zone also observed at Argonne. For the same saturation temperature (283 K), CO_2 had heat transfer coefficients about two to three times those of R-134a. However, no channel dimensions were reported and hence these results are not presently included in our database.

Bao et al. [5] reported local flow boiling coefficients for R-11 and R-123 inside a copper tube with a diameter of 1.95 mm. They used a single piece of tubing, 870 mm long. The first 400 mm of the tube was unheated, providing an entrance region; that section was followed by a 270 mm long test zone and then by a 200 mm unheated exit zone. The tests were conducted in a very thick walled cylinder with external heating elements. For tests over a wide range of conditions (mass velocities from 50 to 1800 kg/m^{2}s, vapor qualities from 0% to 90%, heat fluxes from 5 to 200 kW/m^2 and a range of saturation pressures), they observed that heat transfer coefficients were a strong function of heat flux and increased with

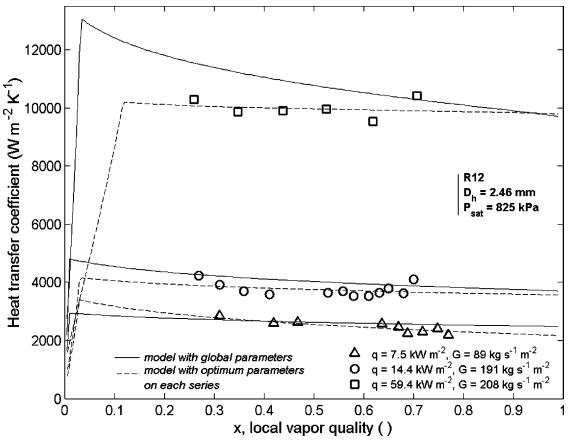

Fig. 3. Flow boiling data for R-12 in 2.46 mm tube of Tran et al. [3].

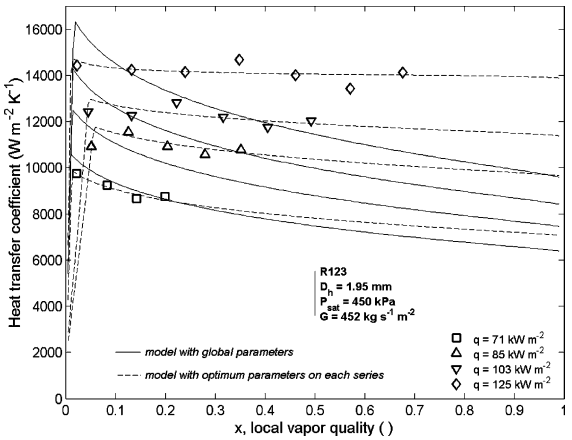

Fig. 5. Flow boiling data for R-123 in 1.95 mm tube of Bao et al. [5].

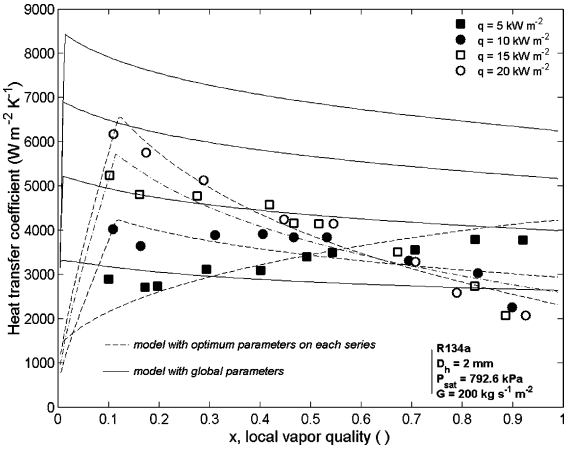

Fig. 4. Flow boiling data for R-134a in 2 mm multi-tube of Yan and Lin [4].

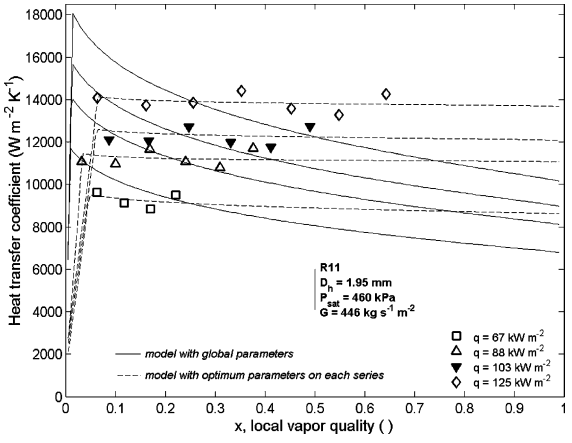

Fig. 6. Flow boiling data for R-11 in 1.95 mm tube of Bao et al. [5].

saturation pressure. However, the effects of vapor quality and mass flux were very small (Figs. 5 and 6). Similar to the previous studies, they concluded that nucleate boiling dominated the heat transfer process. Using the same type of set-up, Baird et al. [6] also reported local heat transfer data for R-123 in a 0.92-mm-diameter tube and CO_2 in the previous 1.95 mm tube, observing the same trends as in their earlier work. Fig. 7 shows some of their local heat transfer coefficients plotted versus vapor quality for CO_2, excluding their subcooled boiling data, for various saturation pressures. Thus, in these tests, the onset of nucleate boiling and hence the formation of the elongated bubbles commenced in the subcooled region. In the heating system used, a copper cylinder with an outside diameter of 25 mm, the thermal inertial of the tube wall is very large in comparison to a single tube with a wall thickness of hundreds of microns.

Lin et al. [7] studied evaporation of R-141b in a vertical 1.1 mm tube over a mass velocity range of 300–2000 kg/m^{2}s and heat flux range of 18–72 kW/m^2, although they only presented data at the mass velocity of 510 kg/m^{2}s. Fig. 8 depicts their results for heat transfer versus vapor quality at these conditions. The outlet pressure of the test section was atmospheric while the inlet pressure varied from 1.34 to 2.19 bar depending the flow conditions, which means the data shown also include a small saturation pressure effect. We were not able to obtain the data from the authors and have estimated the local saturation pressure by a linear interpolation (from the two extreme values given), based on heat flux, to calculate the physical properties to process

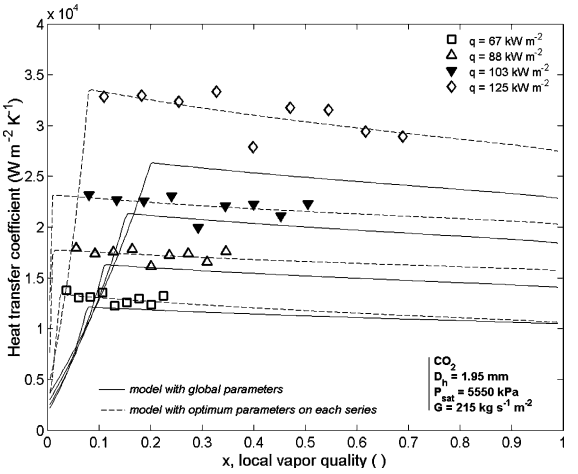

Fig. 7. Flow boiling data for CO_2 in 1.95 mm tube of Baird et al. [6].

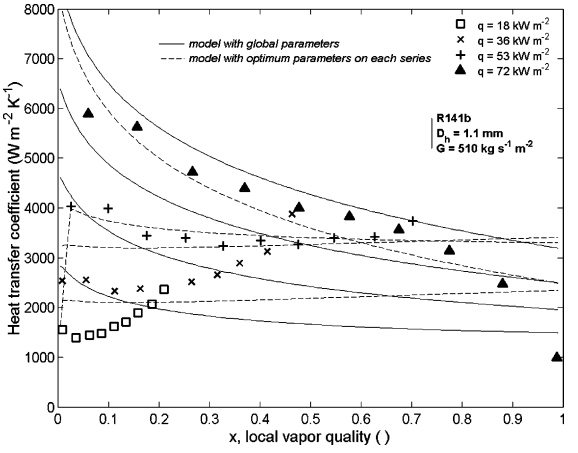

Fig. 8. Flow boiling data for R-141b in 1.1 mm tube of Lin et al. [7].

their data. As opposed to most of the above studies, they found a significant influence of vapor quality on the heat transfer coefficient. At high heat fluxes, their data exhibit a sharp peak at low vapor qualities followed by a monotonic decrease. At low heat fluxes, there was a significant monotonic rise in value up to a peak at about $x = 0.60$. At intermediate heat fluxes, such as 42 and 48 kW/m^2, the heat transfer coefficients were nearly independent of vapor quality as in previous investigations. Hence, these results present a much more complex dependency of the heat transfer coefficient on heat flux and vapor quality than the other studies noted. In the subcooled region, the heat transfer coefficients are much larger than those one would calculated from a single-phase correlation and are similar to the Bao et al. [5] data shown earlier. Consequently, the onset of nucleate boiling and formation of vapor bubbles takes place before the saturated zone, which likely influences the frequency of bubble formation.

Agostini [8] presents multichannel experiment results with R-134a (as Yan and Lin [4]) and it is the only study of the database with two different values of hydraulic diameter, $d_h = 0.77$ mm (18 channels) and 2.01 mm (11 channels) and with rectangular shape of the channel (with smooth corners). The average roughness was measured along the longitudinal axis to be, $Ra = 0.57 \pm 0.01$ μm for the 2.01 mm channels and $Ra = 0.3 \pm 0.1$ μm for the 0.77 mm channels. Heat fluxes ranged from 5.2 to 26.4 kW/m^2 and mass velocities ranged from 117 to 347 kg/m^{2}s. In this test section, the walls were thin and heated by direct electric current. In the case of two-phase flow in the multichannel test section, the uniformity of the mass flow could not be guaranteed. In the case of the 2.01 mm tube, for Boiling number value $Boi < 0.00043$, the author observed that heat transfer coefficients were not sensitive to vapor quality, but beyond a threshold value of x, heat transfer coefficients decreased quickly. For $Boi > 0.00043$, they observed that heat transfer coefficients were not sensitive to vapor quality (Fig. 9), but beyond a threshold value of x heat transfer coefficients increase. These trends are consistent with the results of Lin et al. [7] at low heat flux. In the 0.77 mm tube, the heat transfer coefficients present a peak at a vapor quality between 0.1 and 0.2, independent of the value of heat flux (Fig. 10). These trends are consistent with the results of Lin et al. [7] at high heat flux.

Some general comments are in order about experimental results available for evaporation in microchannels. Most studies have not measured single-phase laminar or turbulent flow heat transfer coefficients prior to their flow boiling tests, which is an important experimental benchmark. Secondly, except for Agostini [8],

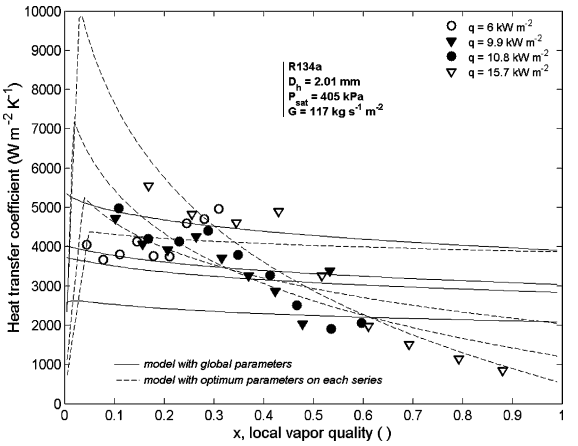

Fig. 9. Flow boiling data for R-134a in 2.01 mm tube of Agostini [8].

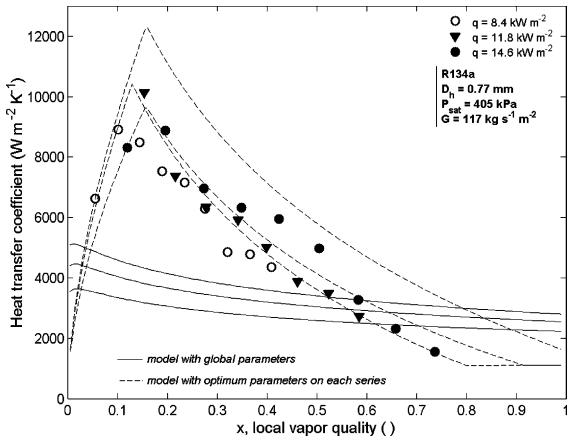

Fig. 10. Flow boiling data for R-134a in 0.77 mm tube of Agostini [8].

the internal surface roughness of the microchannel test sections has not been reported. Third, some studies start with subcooled boiling prior to the test section while some do not, which may or may not significantly influence the saturated zone results. Fourth, achieving steady-state conditions may be an experimental challenge. For instance, Lin et al. [7] noted cyclical temperature fluctuations during their tests. Based on the descriptions, the above experimental heat transfer data are thought to have been measured to accuracies on the order of 5–30% maximum experimental errors depending on the particular test conditions (those quoted in the publications are cited in Table 1), although claims of 5% seem to be optimistic. The physical properties for the test fluids were all obtained from REFPROP version 6.01 of NIST.

Figs. 1–10 make a presentation of the database and comparison with the model are done in the next section.

2. Comparison to heat transfer database

2.1. Description of the parameter identification method

A search for the optimum values of the parameters f, $C_{\delta 0}$ and $\delta_{\min}$ was performed on each series of points of the database. A series is a certain number of experimental points for which the vapor quality changes but the mass velocity, the heat flux and the saturation condition remain constant in the experimental data sets. The least-squared error method was chosen to find the optimum solution $(f, C_{\delta 0}, \delta_{\min})_{\text{opt}}$ i.e. the minimum value of the objective function J defined by:

$$J(f, C_{\delta 0}, \delta_{\min}) = \sum_{i=1}^{n_{\text{serie}}} [h_{\text{exp},i} - h_{\text{model},i}(f, C_{\delta 0}, \delta_{\min})]^2 \qquad (1)$$

The dotted lines on Figs. 1–10 represent the comparison between the experimental series and the evolution given by the model with the $(f, C_{\delta 0}, \delta_{\min})_{\text{opt}}$ corresponding to the specific series. Once the set of optimum values for all the series were determined, they were then used to develop general methods for their prediction, which are presented below.

The optimum values of the identified pair frequency f_{opt}, were found to be strongly dependent on the heat flux in the test section. No clear dependency on any other parameter was identified. Fig. 11 shows f_{opt} versus q for the database, where each point represents one series of experimental points as defined above. For all the fluids and tubes diameters f_{opt} increases with q and a power law was found to give the best fit to the experimental points:

$$f_{\text{opt}} = \left(\frac{q}{q_{\text{ref}}}\right)^{n_f} \qquad (2)$$

The dependency of the pair frequency on the heat flux is consistent with the recent observations of Brutin et al. [11] related to convective boiling of *n*-pentane inside a rectangular channel with a hydraulic diameter of 889 μm and a length of 50 mm. In that study, there appears to be a global increase of the dimensionless frequency of the instabilities related with bubble-generation rate (the transition time in the test section was used as a reference) with the exit vapor quality.

The pair frequency is surmised to be a function of the mass velocity, the geometry and size of the test section,

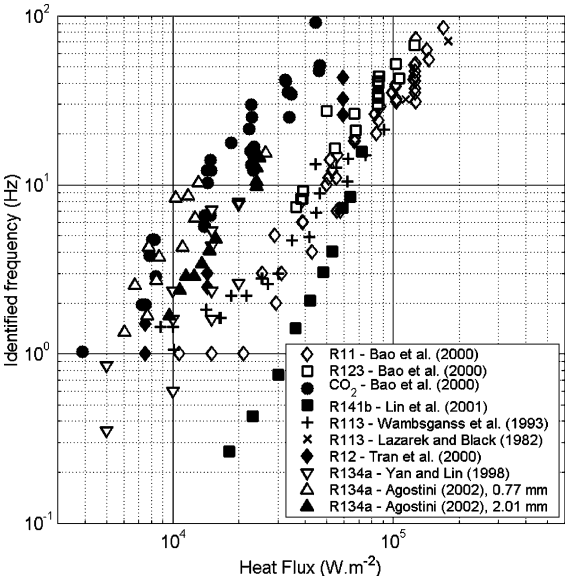

Fig. 11. Evolution of the optimum frequency identified for each series of test versus heat flux for different fluid and tube diameter.

the existence of nucleation sites in relation to roughness and the fluid physical properties. At this time, a predictive law of the bubble frequency based on macroscopic parameters such as q, G and P_{sat} inside a tube of small dimension is not available in the literature. Thus, an empirical relation is proposed based on heat flux only, by introducing values for a reference heat flux and exponent, q_{ref} and n_f, estimated on the entire database. Following the method used by Cooper [12] for his pool boiling correlation, q_{ref} was expressed as a function of the reduced pressure, i.e. the saturation pressure divided by the thermodynamical critical pressure. Indeed, all the physical properties can be expressed as a function of this ratio:

$$q_{ref} = \alpha_q \left(\frac{P_{sat}}{P_{crit}} \right)^{n_q} \tag{3}$$

where α_q is in $W\,m^{-2}$. Fig. 12 shows the values of q_{ref} versus P_{red}, where the horizontal error bar represents the range of reduced pressure for each study. Table 2 summarizes the values of α_q and n_f corresponding to each study. A least squares method on the four parameters $(\alpha_q, n_q, C_{\delta 0}, \delta_{min})$ provides (dotted line law in Fig. 12):

$$q_{ref} = 3328 \left(\frac{P_{sat}}{P_{crit}} \right)^{-0.5} \tag{4}$$

Fig. 13 represents n_f versus q_{ref}. The identified values ranged from 0.7 to 0.8 except for R-134a in Yan and Lin [4] and Agostini [8] for 0.77 mm tube (see Table 2). The best fit on the entire database was obtained with a constant value:

$$n_f = 1.74 \tag{5}$$

Thus, Eqs. (2), (4) and (5) permit the pair (or triplet) frequency to be calculated from the heat flux and the saturation conditions.

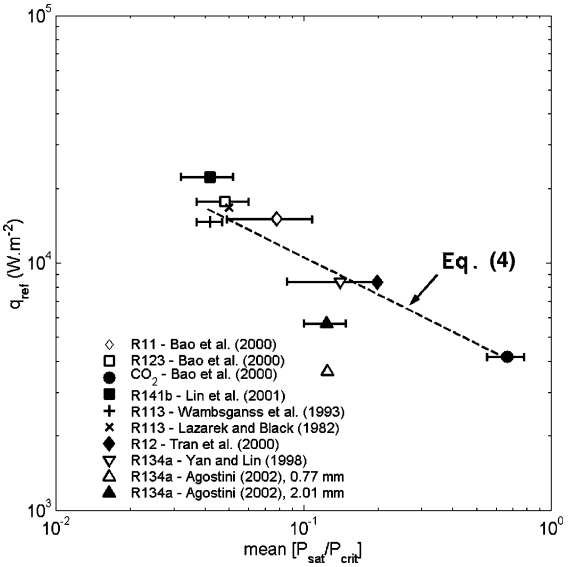

Fig. 12. Evolution of q_{ref} with reduced pressure for each fluids and diameters of the database. The dotted line represents the relation given by Eq. (4).

In the model, a correcting factor on the initial film thickness $C_{\delta 0}$ was added to take into account the change in the fluid properties and the different geometry compared to the original study of Moriyama and Inoue [13] based only on R-113. Fig. 14 shows the mean value of the optimum $C_{\delta 0}$, corresponding to each study of the database versus the reduced pressure. No real relationship to dimensionless numbers or other study parameters could be found. The values ranged from 0.34 to 1.23. The mean correcting factor is 0.84 with a standard deviation of 0.28. This mean value of the correcting factor near unity gives an encouraging sign of the

Table 2
Set of parameters used in the comparison between the model and the database with α_q in $W\,m^{-2}$, δ_{min} in microns and n_q, n_f and $C_{\delta 0}$ are dimensionless

Study	Fluid	Diameter	Specific parameters for each study				
			α_q	n_q	n_f	$C_{\delta 0}$	δ_{min}
Lazarek and Black [1]	R113	3.1	3319	−0.54	1.8	1.176	0.01
Wambsganss et al. [2]	R113	2.92	3298	−0.47	1.72	0.77	0.47
Tran et al. [3]	R12	2.46	3321	−0.57	1.71	0.87	0.36
Yan and Lin [4]	R-134a	2	3551	−0.44	1.27	1.2	1.92
Bao et al. [5]	R11	1.95	3334	−0.59	1.72	0.59	0.02
Bao et al. [5]	R123	1.95	3334	−0.55	1.73	0.44	0.08
Baird et al. [6]	CO_2	1.95	3323	−0.55	1.70	0.34	0.15
Lin et al. [7]	R141b	1.1	3324	−0.60	1.79	0.86	0.58
Agostini [8]	R-134a	0.77	3272	−0.05	1.18	1.23	1.82
Agostini [8]	R-134a	2.01	3452	−0.24	1.70	0.8	3.00
		General model	3328	−0.5	1.74	0.29	0.3

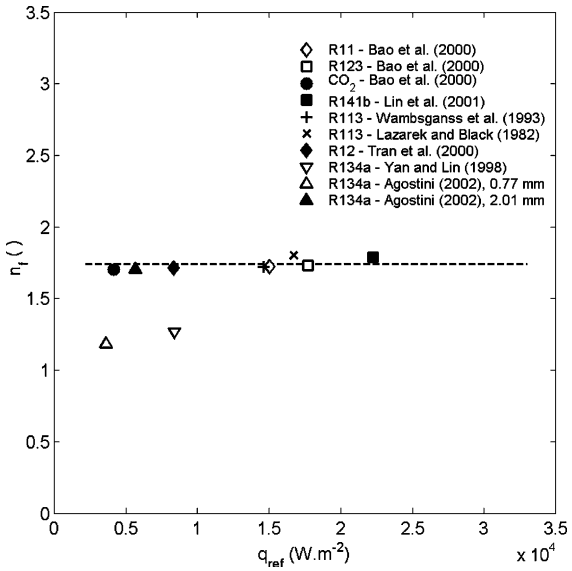

Fig. 13. n_f versus q_{ref} for each fluids and diameters of the database. The dotted line represents the relation given by Eq. (5).

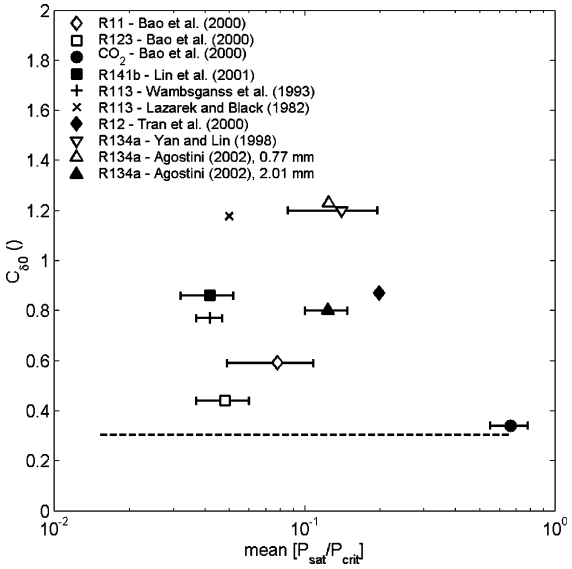

Fig. 14. Optimum values identified for the correcting factor $C_{\delta 0}$ versus reduced pressure for the fluids and diameters of the database. The error bar represents the range of reduced pressure corresponding to each point.

validity of the Eq. (28 of Part I). At this time, no other relation is available for easily determining δ_0 and the Eq. (28 of Part I) is used in our model with a constant value of $C_{\delta 0}$ corresponding to identification on the entire database:

$$C_{\delta 0} = 0.29 \tag{6}$$

Specific studies are needed to measure and better predict with a good accuracy the film formation thickness in microchannels. This goal includes the development of an experimental technique to measure film thicknesses of several microns, which is a challenge today.

The identification of the minimum film thickness using Eq. (43 of Part I) is very difficult due to the sensitive impact of δ_{min} on the mean heat transfer coefficient in the film, i.e. on the final heat transfer coefficient. This high sensitivity is due to the logarithmic ratio δ_0/δ_{min}, i.e. when δ_{min} tends to 0 then h_{film} tends to infinity. In order to reduce this sensitivity of the model to δ_{min}, the mean heat transfer coefficient in the film is calculated by using the average value of the film thickness during t_{film}:

$$h_{film}(z) = \frac{2\lambda_l}{\delta_0(z) + \delta_{min}(z)} \tag{7}$$

In this relation, the weight of δ_{min} is artificially reduced. This expression replaced Eq. (43 of Part I) in finding the optimum parameter values and permits us to calculate the various constants in equations (4)–(7), but no clear trend has been found. Fig. 15 shows the mean values of optimum δ_{min}, corresponding to each database, versus the reduced pressure. The order of magnitude of this minimum thickness of the film is reasonable. Despite the range of values, the above simplified definition of the heat transfer in the film and a sensitivity study suggest the choice of a constant value for δ_{min}, is reasonable, where the choice based on the entire database gives:

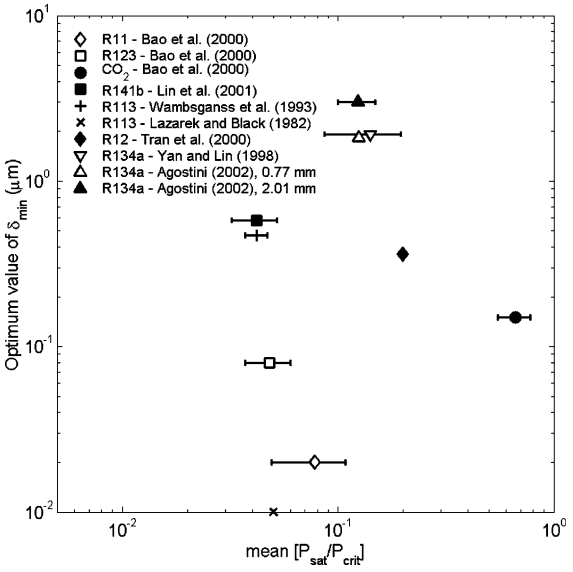

Fig. 15. Optimum values identified for the minimum film thickness δ_{min} versus reduced pressure for the fluids and diameters of the database. The error bar represents the range of reduced pressure corresponding to each point.

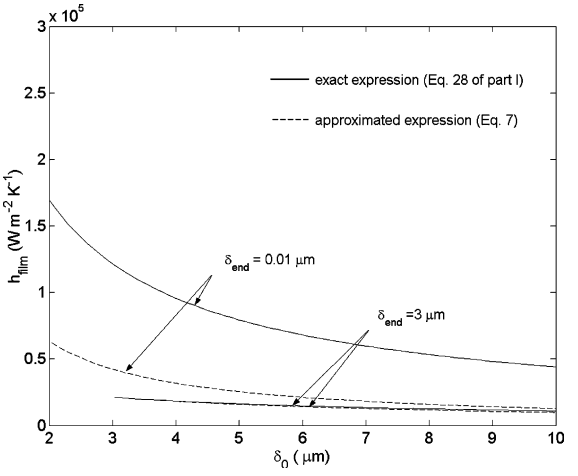

Fig. 16. Comparison between the two methods to calculate the mean heat transfer coefficient in the film. The curves represent the variations of mean heat transfer coefficient in the film versus initial film thickness δ_0 for the two extreme values corresponding to $\delta_{\min}$ in the database.

$$\delta_{\min} = 0.3 \cdot 10^{-6} \text{ m} \tag{8}$$

Considering all the studies, the specific values $\delta_{\min}$ ranged from 0.01 to 3 μm. Fig. 16 shows an example of the difference between the mean heat transfer coefficient in the film calculated using Eqs. (43 of Part I) and (8) with the thermal conductivity of the R-134a. When the value of $\delta_{\min}$ is of the same order of magnitude as δ_0 ($\delta_{\text{end}} = 3$ μm), then the two solutions are close; however, when $\delta_{\min}$ is two orders of magnitude below that of δ_0 ($\delta_{\text{end}} = 0.01$ μm), a significant underprediction of h_{film} occurs when Eq. (7) is used. The simplification offered by Eq. (8) gives more weigh to values of $\delta_{\min}$ around one micron (which in fact is the order of magnitude of the roughness that breaks the film as shown previously in Part I). It gives a reasonable approximation of the mean heat transfer in this case.

2.2. Comparison of the model with the experimental trends

Figs. 1–10 present the evolution of the heat transfer coefficients versus the vapor quality in comparison to predictions by the model with several experimental series from the database. Two comparisons are presented. The model run with the best set of values $(f, C_{\delta 0}, \delta_{\min})$ corresponding to each series (dotted lines), which in fact can be significantly different from the specific parameters of the study listed in Table 2. The "plain" line represents the variation of h calculated with the general values of parameters given by the Eqs. (6)–(8). The values of G, q, P_{sat}, and d_{h} used in the calculations are listed on the graphs.

In the case of small variations of h with x, i.e. for Lazarek and Black [1], Wambsganss et al. [2], Tran et al. [3], Bao et al. [5] and Baird et al. [6], the model with series specific parameters shows very good agreement with the experimental results. If the general values of $C_{\delta 0}$ and $\delta_{\min}$ are used, the difference between model and experiment can be significant, particularly with the results of Wambsganss et al. [2] in Fig. 2. This deviation is directly related to the scattering of the specific values of each series around the global parameters, but the trends are still correct. In our model for low vapor quality, the heat transfer increases strongly up to its peak where local dryout occurs, where $\delta = \delta_{min}$. After the peak, the local heat transfer decreases because of (i) the increase of the dryout period and the poor heat transfer from the dry wall in the heat transfer cycle and (ii) decrease of the initial film thickness δ_0 with the increase of the two-phase flow velocity with increasing x, i.e. earlier dryout.

In the case of large variations of h with x, such as in multichannel studies of Yan and Lin [4], Agostini [8] or in the single tube study of Lin et al. [7], the results are variable from one study to another. For Yan and Lin [4], the model with specific parameters gives good trends, especially for the difference in behavior linked with the heat flux. For $q = 5$ kW m^{-2}, in our model h grows with vapor quality because local dryout does not occur. In this case, delay of the onset of local dryout permits the heat transfer coefficient to increase until vapor qualities up to 0.6 and then falls beyond this value. The model with the general parameters is not able to gives this change in trends and the deviation between the model and experiment increases dramatically. Considering the studies of Lin et al. [7] and Agostini [8], the same analyses could be done and the deviations are also notable.

2.3. Comparison of the model with specific parameters with the database

In Fig. 17, the model with the four specific parameters, corresponding to each study (Table 2), is compared to the experimental points. This version of the model predict 90% of the data to within ±30% and the deviation decreases with increasing values of the heat transfer coefficient for $h > 6000$ W m^{-2} K^{-1}. In order to show the contribution of each study on this global result, the cumulated number of experimental points has been plotted versus the deviation in Fig. 18. Values for a series is plotted to show what percent of the points in that series is within a specific percent deviation. The grey line represents the distribution for the entire database and the studies below this line correspond to the worst results, which correspond to the multichannel studies. It is difficult to reject these studies from the current study even if our model does not specifically pertain to any additional factors influencing evaporation inside multichannels, such as maldistribution or flow oscillations.

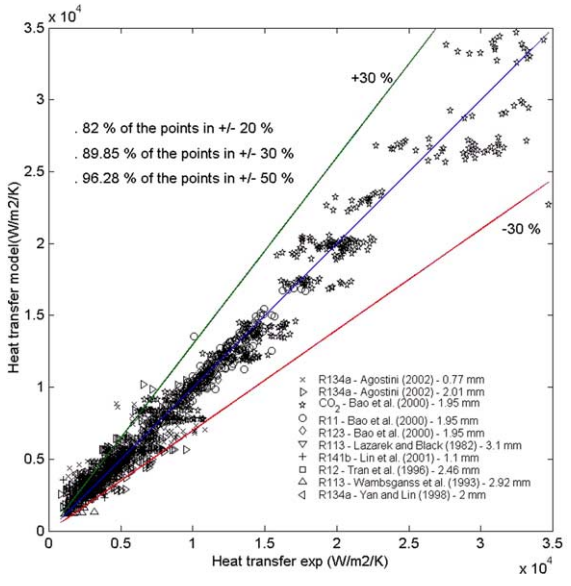

Fig. 17. Comparison between experimental heat transfer and the corresponding values given by the model with different constant values of α_q, n_q, n_f, $C_{\delta 0}$ and δ_{min}, resulting from an optimisation on each database.

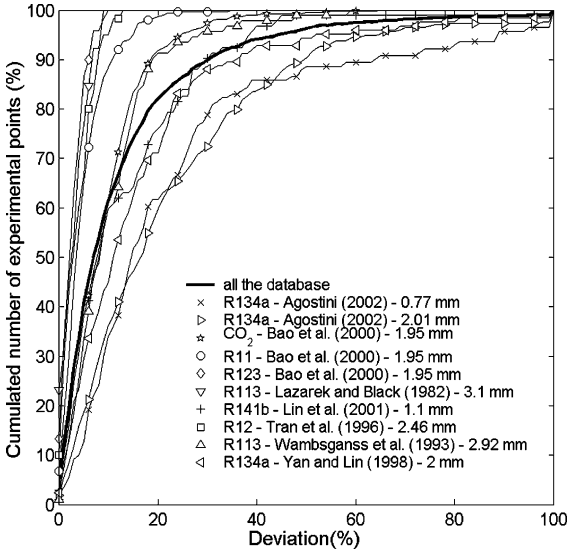

Fig. 18. Distribution of the rate of experimental points as a function of the deviation between the heat transfer coefficient calculated with optimised constant values of α_q, n_q, n_f, $C_{\delta 0}$ and δ_{min}, and the heat transfer coefficient from the different databases.

The type of fluid, R-134a, common to all the multichannel experiments could also be invoked. Without considering the multichannel experiments in the database, the model with specific parameters predicts 98% of the data to ±30%.

2.4. Comparison of the global model with the database

In Fig. 19, the model with its general parameters is compared to the experimental data. This general model predicts 70% of the points to ±30%. With this version of the model, again the deviation increases for low values of the heat transfer coefficient. Fig. 20 shows the

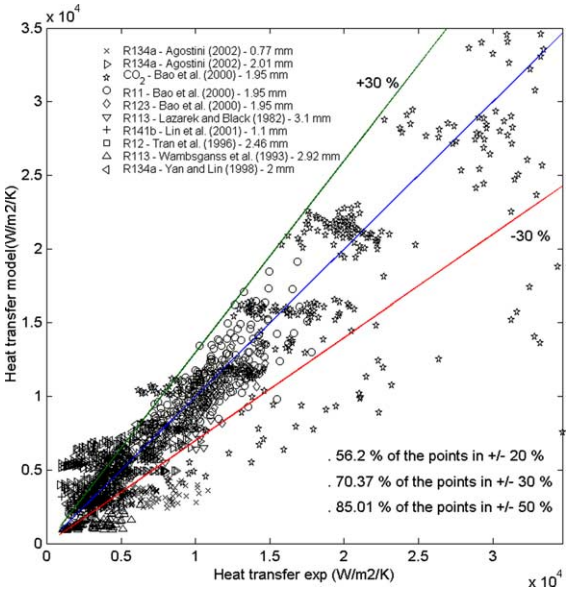

Fig. 19. Comparison between experimental heat transfer and the corresponding values given by the model using the general values of α_q, n_q, n_f, $C_{\delta 0}$ and δ_{min}.

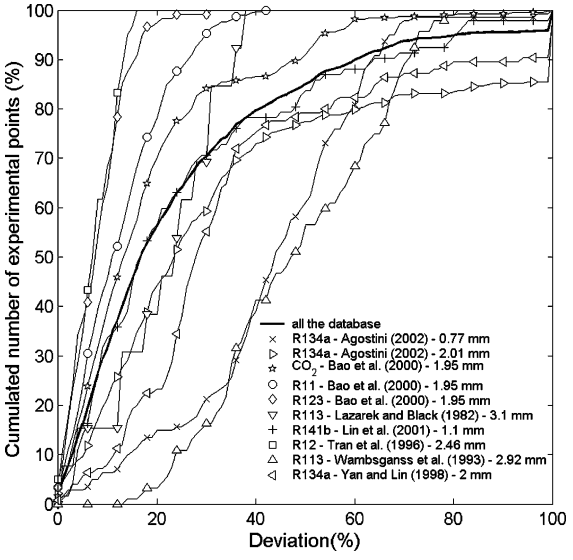

Fig. 20. Deviation between the data and the model using the general value of α_q, n_q, n_f, $C_{\delta 0}$ and δ_{min}.

cumulated number of experimental points versus the deviation. The multichannel studies and the data from Wambsganss et al. [2] are, again, poorly described. In summary, without the multichannel experiments in the database, the general model predicts 83% of the data to ±30%. This performance is promising considering the difficulty in accurately measuring heat transfer coefficients in microchannels, the variety of measurement methods applied, the effects of inlet subcooling on the pair frequency, unknown surface roughness and so forth. In reality, microchannel two-phase flows are susceptible to instabilities and there is typically observed a variation in length of elongated bubbles, points which have not yet been addressed in the model.

The unexpected good agreement for the CO_2 is due to the fact that intermittent and annular flows are present over a wide range of vapor quality according to Pettersen [14]. These flow regimes are similar to elongated bubble in the model, and an equivalent frequency and an initial film thickness can be identified.

3. Simulations with the new model

In that section, the calculations were all run using the general parameter values in the model.

3.1. Influence of d on the heat transfer coefficient

In order to illustrate the influence of tube diameter, the model has been run with R-123 at $P_{sat} = 350$ kPa, $G = 120\ \mathrm{kg\,m^{-2}\,s^{-1}}$ and $q = 100\ \mathrm{kW\,m^{-2}}$. Fig. 21 shows the heat transfer coefficient versus the vapor quality for diameters ranging from 0.5 to 2 mm in increments of 0.166 mm and Fig. 22 shows h versus d for values of x ranging from 0.1 to 0.9 in increments of 0.1. There are three effects: for $x < 0.04$, h decreases with d, then for $x > 0.18$, h increases with d, and for $0.04 < x < 0.18$ the heat transfer coefficient increases, reaches a peak, and afterwards decreases with d. Depending on the thermophysical properties of the fluid and the operating conditions, each zone could disappear or move. In the model, the influence of the diameter is directly linked with the equation (28 of Part I) that gives the initial film thickness δ_0. Fig. 23 illustrates this dependence with δ_0 plotted versus d for two representative pair velocities. Increasing the diameter results in a thicker initial film and thus the onset of the periodical dryout is shifted to a higher vapor quality. On the other hand, increasing the velocity decreases δ_0.

The limited number of experiments that show a diameter effect do not permit one to deduce a clear trend. For example, Yan et al. [4] concluded that evaporation heat transfer in a small pipe is more effective than in a larger pipe, when passing from macro to microscale tubes. But what happens when the diameter

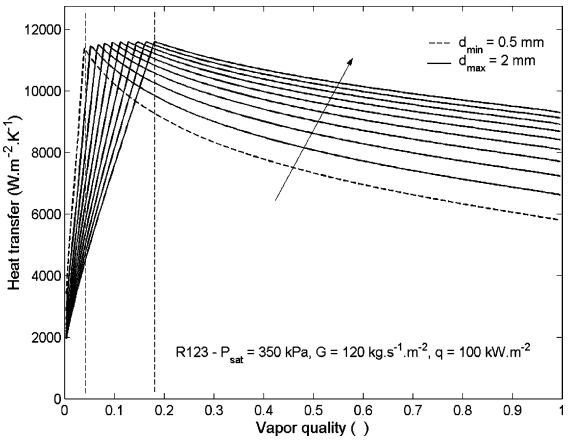

Fig. 21. Heat transfer coefficient versus vapor quality for different diameters (increment of 0.166 mm).

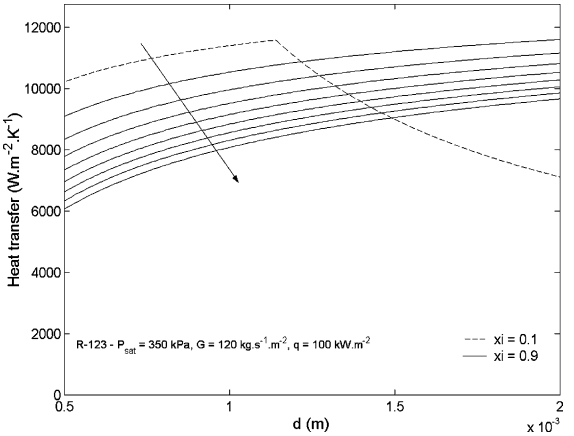

Fig. 22. Heat transfer coefficient versus diameter for different vapor qualities (increment of 0.088).

is decreased within the microscale? For R-134a in multichannels, for diameters of 0.77 and 2.01 tubes, at a mass velocity of 285 $\mathrm{kg\,m^{-2}\,s^{-1}}$, the data of Agostini [8] show a higher heat transfer coefficient for the small tube but only for $x < 0.25$. For R-142b, Palm [15] shows a moderate increase of h when d decreases in 3.5, 2.5, 1.5 and 1mm tubes. Using the criteria of Kew and Cornwell [16], based on $Co = 0.5$, the threshold diameter for micro-macroscale transition equals 2.14 mm for R-142b at 15 °C. Of course, the reliability of this criterion has not yet been established, but these results seem to be representative of the increase of the heat transfer coefficient in the micro-macroscale transition zone. For R-134a, Owhaib and Palm [17] at 645 kPa found that the average heat transfer coefficient increases when the diameter decreased from 1.7 mm to 0.8 mm. In this case, the threshold diameter is 1.68 mm and we can

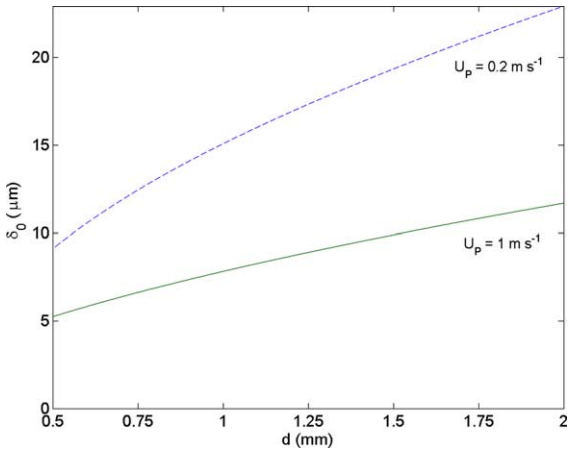

Fig. 23. Initial film thickness versus hydraulic diameter.

reasonably assume these results correspond to micro-scale, but the method used to define the average coefficient (on mass flux and/or vapor quality) is not specified. These results seem to correspond to vapor qualities below 0.4. For R-123, Baird et al. [6] have tested 0.92 and 1.95 mm and affirm that diameter has no significant effect on h. They proposed a correlation independent of the diameter to predict h. The threshold diameter for this last fluid is 1.78 mm, once again the results correspond to the micro-macroscale transition. Khodabandeh [18] studied the heat transfer coefficient of an advanced two-phase thermosiphon with isobutene as refrigerant with tube diameter ranging from 1.1 to 6 mm. He concluded that the influence of d is small and no clear trend could be seen.

Fig. 24 shows the comparison between the model and the data of Baird et al. [6]. The vapor quality chosen corresponds to the mean value of x of their experimental points, $x = 0.255$. The two extreme values of the range of mass flux $G = 167.4$ and 337.6 kg m^{-2} s^{-1} were used with the 1.95 mm tube (dotted lines) and $G = 450$ kg m^{-2} s^{-1} with the 0.92 mm tube (from [6] only data for CO_2 in 1.95 mm tube are include in the database). The model predicts an increase of the heat transfer coefficient with a decrease of the diameter below a heat flux of 18 kW m^{-2}. Beyond this threshold value of q, decreasing of the diameter should give a significant decrease in h. Unfortunately, the different ranges of heat flux corresponding to the two diameters in these experiments do not permit this expectation to be verified, but the predictions of the model are compatible with the trends in this case. Notice that this threshold value of the heat flux is only due to the different values G used for each diameter calculation.

3.2. Influence of q on the heat transfer coefficient

Fig. 25 shows the heat transfer coefficient as a function of the vapor quality for R-12 at $P_{sat} = 825$ kPa, $G = 200$ kg m^{-2} s^{-1} and for heat flux ranging from 60 to 120 kW m^{-2} in increments of 6.66 kW m^{-2}. This case illustrates that both heat flux and vapor quality could influence the heat transfer coefficient. The vapor quality effect can be divided into three zones. In the first zone, for $x < 0.12$, the model predicts an increase in the heat transfer coefficient with q. This trend is inverted in zone 2 ($0.12 < x < 0.38$). The lower limit of zone three corresponds to the first peak in h (for this given range of q) where dryout occurs cyclically. The peak in h is shifted to higher values of vapor quality when q increases, i.e. the local dryout occurs later for higher q. The relation between the frequency of the pairs and the heat flux can explain this surprising result (Eq. (2)); when q increases

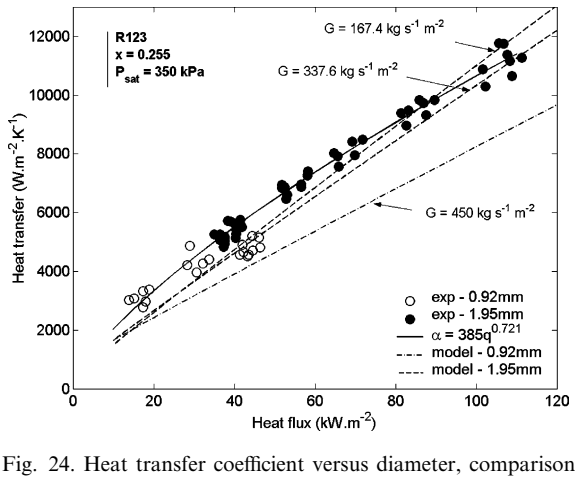

Fig. 24. Heat transfer coefficient versus diameter, comparison with Baird et al. [6].

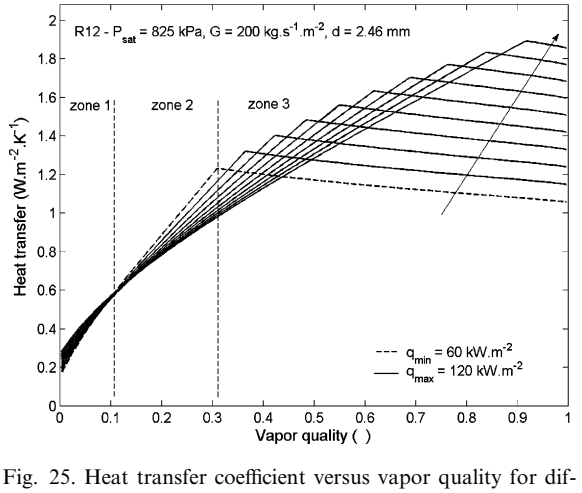

Fig. 25. Heat transfer coefficient versus vapor quality for different values of the heat flux (increment of 6.66 kW m^{-2}).

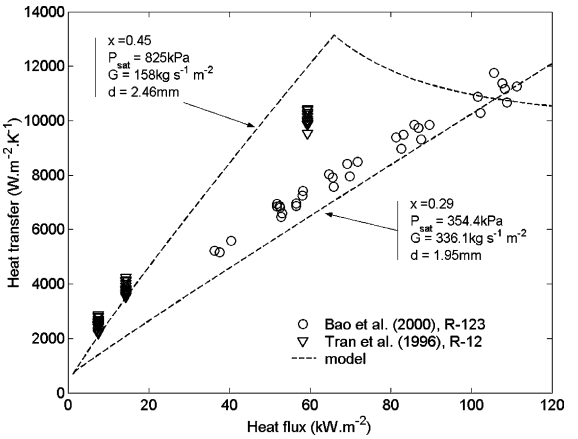

Fig. 26. Heat transfer coefficient versus heat flux, comparison with Bao et al. [5].

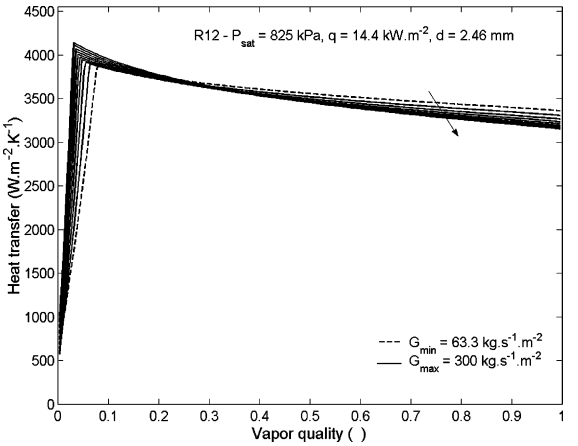

Fig. 27. Heat transfer coefficient versus vapor quality for different values of the mass velocity (increment of 26.3 kg m^{-2} s^{-1}).

the maximum film duration $t_{\text{dry film}}$ decreases but the vapor duration t_v decreases due to the increase of the frequency. In zone three, at a given value of x, h rises and decreases with q.

Fig. 26 shows the heat transfer coefficient plotted versus heat flux, comparing the results of the model and the experiments of Bao et al. [5] for R-123 with $P_{\text{sat}} = 354$ kPa, $G = 336$ kg m^{-2} s^{-1} and x ranging from 0.05 to 0.85, and Tran et al. [3] for R-12 with $P_{\text{sat}} = 825$ kPa, G ranging from 63 to 300 kg m^{-2} s^{-1} and x ranging from 0.2 to 0.77. The model predicts reasonably well the improvement of h with q. As described above, the enhancement of h is due to the effect of the heat flux on the frequency; however, for high heat flux, for R-12 with $q > 70$ kW m^{-2}, the increase of $t_{\text{dry film}}$ is not counterbalanced by the decrease of t_v. To date such a decrease beyond a certain heat flux has not been observed experimentally and this predicted trend must be considered with caution.

3.3. Influence of G on the heat transfer coefficient

Nearly all the studies point out the lack of influence of the mass velocity on the heat transfer coefficients and Bao et al. [5] suggested that this independence is due to the small contribution of the convective heat transfer coefficient on the overall coefficient. Fig. 27 represents the predicted heat transfer coefficient versus vapor quality for R-12 at mass velocities ranging from 63.3 to 300 kg m^{-2} s^{-1}. The saturation condition corresponds to Tran et al. [3]; $P_{\text{sat}} = 825$ kPa, $q = 14.4$ kW m^{-2}. The effect of the mass velocity is negligible over a large range of x, i.e. the model based on film evaporation is able to catch the small influence of G. In our model, G influences the onset of the local dry-out because an increase in G results in a decrease of the initial film thickness as described in Fig. 23.

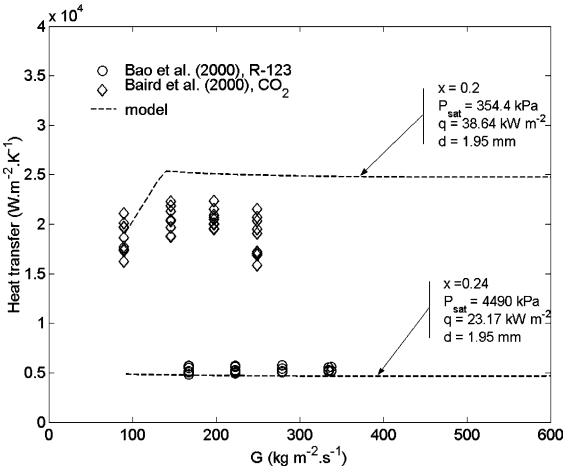

Fig. 28. Heat transfer coefficient versus mass velocity, comparison with Bao et al. [5].

Fig. 28 shows h versus G in comparison to the experimental results of Bao et al. [5] for R-123, with P_{sat} ranging from 348 to 360 kPa, q ranging from 36.26 to 41.83 kW m^{-2}, and x ranging from 0.019 to 0.558, and Baird et al. [6] for CO_2, with P_{sat} ranging from 4331 to 4459 kPa, q ranging from 22.17 to 24.72 kW m^{-2}, and x ranging from 0.041 to 0.687. For R-123, the impact of G is negligible and for CO_2 heat transfer decreases slightly. Thus, experimentally a very large range of mass velocities seems to be necessary to observe an influence of G.

3.4. Influence of P_{sat} on the heat transfer coefficient

Fig. 29 presents h versus vapor quality, for R-123 at $q = 14.4$ kW m^{-2} and $G = 334.8$ kg m^{-2} s^{-1} for different values of the saturation pressure ranging from 600 to

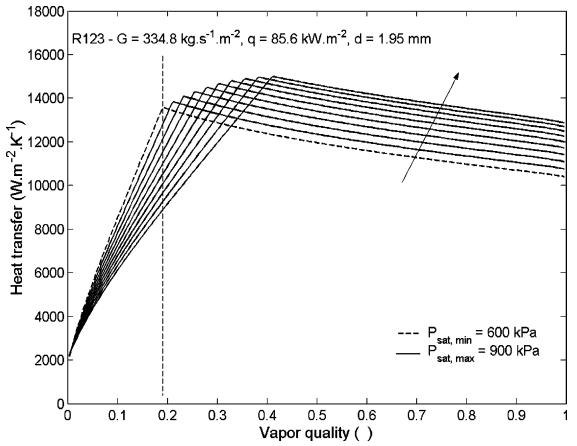

Fig. 29. Heat transfer coefficient versus vapor quality for different values of the saturation pressure.

900 kPa, in increments of 33.3 kPa. Before the threshold value of cyclical dryout, the heat transfer coefficient increases, reaches a peak and afterwards decreases with rising x. Increasing the pressure shifts the cyclical dryout location to the higher values of x. When the pressure increases, the liquid density and the latent heat of vaporization both decrease, so that from Eq. (33 of Part I) the vaporisation of the film is promoted. Inversely, from (2) it appears that the frequency of the pair increases with P_{sat} and thus onset of dryout is delayed. This last mechanism explains the trends in Fig. 29.

Fig. 30 presents a comparison between the model and experimental data for the heat transfer coefficient versus P_{sat}. For R-123, the model predicts reasonably well the data from Bao et al. [5] with $G = 334.8\ \mathrm{kg\,m^{-2}\,s^{-1}}$, q ranging from 81.2 to 91.3 $\mathrm{kW\,m^{-2}}$ and x ranging from 0.02 to 0.64. In this case, the model predicts a decrease of h up to 800 kPa, due the mechanisms explained above. For R-134, the agreement with the data from Yan and Lin [4] is poor, with $G = 100\ \mathrm{kg\,m^{-2}\,s^{-1}}$, $q = 5\ \mathrm{kW\,m^{-2}}$ and x ranging from 0.09 to 0.93, but this is a multichannel where additional effects ignored here in our single channel model may come into play.

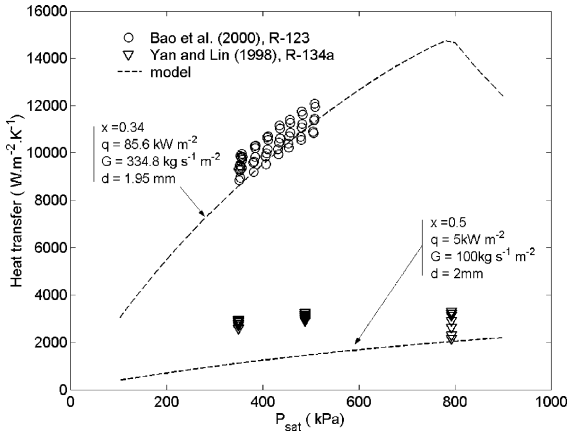

Fig. 30. Heat transfer coefficient versus saturation conditions, comparison with Bao et al. [5] and Yan and Lin [4].

4. Conclusions

A *three-zone* flow boiling model has been presented to describe evaporation of elongated bubbles in microchannels. The heat transfer model predicts the transient variation in local heat transfer coefficient during the cyclic passage of (i) a liquid slug, (ii) an evaporating elongated bubble and (iii) a vapor slug when present. A time-averaged local heat transfer coefficient is thus obtained and is compared to experimental data taken from seven independent studies covering the following seven fluids: R-11, R-12, R-113, R-123, R-134a, R-141b and CO_2. The 1591 test data covered tube diameters from 0.77–3.1 mm, mass velocities from 50 to 564 $\mathrm{kg/m^2 s}$, heat fluxes from 5 to 178 $\mathrm{kW/m^2}$ and vapor qualities from 0.01 to 0.99. The new model predicts 70% of the database to within ±30%.

The new model successfully predicts the trends in the heat transfer data, including the expected effects of vapor quality, heat flux, mass velocity, saturation pressure and tube diameter. The peak noticeable in some data sets at low vapor quality, for instance, has been shown to occur when dryout of the liquid film at the end of elongated bubbles occurs before the arrival of the next liquid slug.

Acknowledgements

A.M. Jacobi received partial support for this project as an ERCOFTAC Scientific Visitor to the Laboratory of Heat and Mass Transfer at the EPFL in Lausanne. B.S. Haynes from the Department of Chemical Engineering of the University of Sydney, Australia kindly provided their experimental database.

References

[1] G.M. Lazarek, S.H. Black, Evaporative heat transfer, pressure drop and critical heat flux in a small vertical tube with R-113, Int. J. Heat Mass Transfer 25 (7) (1982) 945–960.

[2] M.W. Wambsganss, D.M. France, J.A. Jendraejczyk, T.N. Tran, Boiling heat transfer in a horizontal small-diameter tube, J. Heat Transfer 115 (1993) 963–972.

[3] T.N. Tran, M.W. Wambsganss, D.M. France, Small circular and rectangular channel boiling with two refrigerants, Int. J. Multiphase Flow 22 (3) (1996) 485–498.

[4] Y.Y. Yan, T.F. Lin, Evaporation heat transfer and pressure drop of refrigerant R-134a in a small pipe, Int. J. Heat Mass Transfer 41 (1998) 4183–4194.
[5] Z.Y. Bao, D.F. Fletcher, B.S. Haynes, Flow boiling heat transfer of freon R11 and HFCFC123 in narrow passages, Int. J. Heat Mass Transfer 43 (2000) 3347–3358.
[6] J.R. Baird, Z.Y. Bao, D.F. Fletcher, B.S. Haynes, Local flow boiling heat transfer coefficients in narrow conduits. In: Bar-Cohen, A. (Ed.), Boiling 2000: Phenomena and Engineering Applications, vol. 2, Anchorage Alaska, Apr 30–May 5, 2000, pp. 447–466.
[7] S. Lin, P.A. Kew, K. Cornwell, Two-phase heat transfer to a refrigerant in a 1 mm diameter tube, Int. J. Refrig. 24 (2001) 51–56.
[8] B. Agostini, Etude expérimentale de l'ébullition de fluide réfrigérant en convection forcée dans des mini-canaux, Ph.D. Thesis, Université Joseph Fourier, Grenoble, France, 2002.
[9] R. Webb, J.W. Paek, Discussion on Evaporation heat transfer and pressure drop of refrigerant R-134a in a small pipe, Int. J. Heat Mass Transfer 46 (2003) 1111–1113.
[10] Y. Zhao, M. Molki, M.M. Ohadi, S.V. Dessiatoun, Flow boiling of CO_2 in microchannels, ASHRAE Trans. 106 (1) (2000) 437–445.
[11] D. Brutin, F. Topin, L. Tadrist, Experimental study of unsteady convective boiling in heated minichannels, Int. J. Heat Mass Transfer 46 (2003) 2957–2965.
[12] M.G. Cooper, Heat flow rate in saturated nucleate pool boiling—a wide-ranging examination using reduced properties, Advances in Heat Transfer, vol. 16, Academic Press, Orlando, 1984, pp. 157–239.
[13] K. Moriyama, A. Inoue, Thickness of the liquid film formed by a growing bubble in a narrow gap between two horizontal plates, J. Heat Transfer 118 (1996) 132–139.
[14] J. Pettersen, Two-phase flow pattern during microchannel vaporization of CO_2 at near-critical pressures. In: Proceedings of First ASME International Conference on Microchannels and Minichannels, Rochester, New York, 2003, pp. 93–102.
[15] B. Palm, Mini-and Microchannel Research in Sweden. In: Proceedings of First ASME International Conference on Microchannels and Minichannels, Rochester, New York, 2003, pp. 25–31.
[16] P.A. Kew, K. Cornwell, Correlations for the prediction of boiling heat transfer in small-diameter channels, Appl. Thermal Eng. 17 (8–10) (1997) 705–715.
[17] W. Owhaib, B. Palm, Flow Boiling Heat Transfer in a vertical circular microchanneltube, Eurotherm Seminar No. 72, Valencia, Spain, 31 March–2 April, 2003.
[18] R. Khodabandeh, Influence of channel diameter on boiling heat transfer in a closed advanced two-phase thermosiphon loop. In: Proceedings of 5th International Boiling Conference in Montego Bay, Jamaica, May 4–8, 2003.